Physics in Medicine & Biology

IPEM Institute of Physics and Engineering in Medicine

PAPER • OPEN ACCESS

Theoretical and experimental characterization of novel water-equivalent plastics in clinical high-energy carbon-ion beams

To cite this article: A Lourenço *et al* 2016 *Phys. Med. Biol.* **61** 7623

OPEN ACCESS
IOP Publishing | Institute of Physics and Engineering in Medicine Physics in Medicine & Biology
Phys. Med. Biol. **61** (2016) 7623–7638 doi:10.1088/0031-9155/61/21/7623

Theoretical and experimental characterization of novel water-equivalent plastics in clinical high-energy carbon-ion beams

A Lourenço[1,2], N Wellock[3], R Thomas[2], M Homer[2], H Bouchard[4], T Kanai[5], N MacDougall[3], G Royle[1] and H Palmans[2,6]

[1] Department of Medical Physics and Biomedical Engineering, University College London, London WC1E 6BT, UK
[2] Division of Acoustics and Ionising Radiation, National Physical Laboratory, Teddington TW11 0LW, UK
[3] Clinical Physics, St Bartholomew's Hospital, Barts Health NHS Trust, London EC1A 7BE, UK
[4] Département de Physique, Université de Montréal, Pavillon Roger-Gaudry, 2900 Boulevard Edouard-Montpetit, Montréal, Québec, H3T 1J4, Canada
[5] Gunma University Heavy Ion Medical Center, Gunma University, Showa 3-39-22, Maebashi, Gunma 371-8511, Japan
[6] Medical Physics Group, EBG MedAustron GmbH, A-2700 Wiener Neustadt, Austria

E-mail: am.lourenco@ucl.ac.uk

Received 13 May 2016, revised 31 August 2016
Accepted for publication 22 September 2016
Published 14 October 2016

Abstract

Water-equivalent plastics are frequently used in dosimetry for experimental simplicity. This work evaluates the water-equivalence of novel water-equivalent plastics specifically designed for light-ion beams, as well as commercially available plastics in a clinical high-energy carbon-ion beam. A plastic-to-water conversion factor $H_{pl,w}$ was established to derive absorbed dose to water in a water phantom from ionization chamber readings performed in a plastic phantom. Three trial plastic materials with varying atomic compositions were produced and experimentally characterized in a high-energy carbon-ion beam. Measurements were performed with a Roos ionization chamber, using a broad un-modulated beam of $11 \times 11\,cm^2$, to measure the plastic-to-water

conversion factor for the novel materials. The experimental results were compared with Monte Carlo simulations. Commercially available plastics were also simulated for comparison with the plastics tested experimentally, with particular attention to the influence of nuclear interaction cross sections. The measured $H_{\mathrm{pl,w}}^{\mathrm{exp}}$ correction increased gradually from 0% at the surface to 0.7% at a depth near the Bragg peak for one of the plastics prepared in this work, while for the other two plastics a maximum correction of 0.8%–1.3% was found. Average differences between experimental and numerical simulations were 0.2%. Monte Carlo results showed that for polyethylene, polystyrene, Rando phantom soft tissue and A-150, the correction increased from 0% to 2.5%–4.0% with depth, while for PMMA it increased to 2%. Water-equivalent plastics such as, Plastic Water, RMI-457, Gammex 457-CTG, WT1 and Virtual Water, gave similar results where maximum corrections were of the order of 2%. Considering the results from Monte Carlo simulations, one of the novel plastics was found to be superior in comparison with the plastic materials currently used in dosimetry, demonstrating that it is feasible to tailor plastic materials to be water-equivalent for carbon ions specifically.

Keywords: carbon-ion radiotherapy, water-equivalent plastics, relative dosimetry, conversion factors

(Some figures may appear in colour only in the online journal)

1. Introduction

In the most recent international codes of practice for the dosimetry of radiotherapeutic carbon-ion beams (Vynckier *et al* 1991, Andreo *et al* 2000), water is the recommended medium for the determination of absorbed dose. However, for relative dosimetry, for quality assurance (QA) of reference and relative dosimetry and for treatment planning verification, water- or tissue-equivalent plastic materials are often used in the measurements for convenience of realizing the setup.

The water-equivalence and tissue-equivalence of phantom materials in light-ion beams is widely considered to be related to stopping powers and ranges (Zhang *et al* 2010, Kanematsu *et al* 2013). It is, however, also substantially influenced by the nuclear interaction cross sections, though this mechanism is less well quantified and understood. Nuclear interactions have important consequences on primary dosimetry using non-water calorimeters (Palmans *et al* 2013, Rossomme *et al* 2013), reference and relative dosimetry in plastic water-substitute phantoms and dose verification in complex, anatomic and anthropomorphic phantoms (Palmans *et al* 2002). Their importance has also been demonstrated for the comparison of dose calculations in tissue and in water (Palmans and Verhaegen 2005, Paganetti 2009). For carbon-ion beams, Inaniwa *et al* (2015a, 2015b) investigated the influence of nuclear interactions on dose calculations in treatment planning. The effects were tumour site, fraction size and patient dependent and could be substantial in particular cases. Kanematsu *et al* (2014) calculated and experimentally verified the impact of using polyethylene range compensators on the spread-out Bragg peak (SOBP) dose in carbon-ion beams, with particular attention to the influence of nuclear interactions. They reported corrections of 3% in extreme cases when a range compensator of 20 cm needs to be used and a correction of the order of 1% in most clinical cases.

Palmans and Verhaegen (1997) indicated that the main source of differences in the shape of the Bragg peak between low-Z materials is due to differences in the non-elastic nuclear interaction cross sections. In light-ion beams, the difference of non-elastic nuclear interactions between different elements results in different particle fluences between water and plastic materials at equivalent depths. Palmans *et al* (2002) established a fluence correction factor, k_{fl}, to account for those differences. They calculated fluence corrections for PMMA and polystyrene with reference to water in low- and high-energy clinical proton beams using the PTRAN Monte Carlo code and experimental data. While for low-energy beams fluence corrections were smaller than 1%, for high-energy beams corrections were of the order of 2%–5%. With regards to the fluence correction factor for carbon-ion beams, fewer studies have been carried out compared to electron and proton beams (Khan *et al* 1991, Palmans *et al* 2002, 2013, Al-Sulaiti *et al* 2010, 2012, Lourenço *et al* 2016). Lühr *et al* (2011a) performed a Monte Carlo study, using SHIELD-HIT10A, to determine fluence corrections for PMMA, bone and graphite in comparison to water in carbon-ion and proton beams. Rossomme *et al* (2013) conducted an experimental and numerical comparison of k_{fl} between water and graphite for a low-energy carbon-ion beam, which is important for the conversion to dose to water for graphite calorimetry.

To convert ionization chamber readings in a plastic phantom to the equivalent reading in a water phantom, the IAEA TRS-398 Code of Practice (Andreo *et al* 2000) established a fluence scaling factor, h_{pl}. Thwaites (1985) calculated fluence scaling factors between water and plastic phantoms for electron beams. The results showed that measured values of h_{pl} were dependent on the ionization chamber and beam energy. This has been further investigated by Ding *et al* (1997) for clear polystyrene, white polystyrene and PMMA phantom materials and by McEwen and DuSautoy (2003) for the water-equivalent material WTe. For photon beams, Seuntjens *et al* (2005) conducted a study to measure the h_{pl} factor in six water-equivalent plastics.

In this work, we discuss the water-equivalence of three novel plastic materials developed specifically for light-ion beam dosimetry, with particular attention to the influence of nuclear interaction cross sections. A plastic-to-water conversion factor, $H_{\mathrm{pl,w}}$, was established to derive absorbed dose-to-water in a water phantom from ionization chamber readings performed in a plastic phantom, in a similar way as was previously proposed for electron and photon beams (Ding *et al* 1997, McEwen and DuSautoy 2003, Seuntjens *et al* 2005). This study also derives a relation between $H_{\mathrm{pl,w}}$, h_{pl} and k_{fl}. The novel materials were experimentally characterized at the Gunma University Heavy Ion Medical Center, Japan, using a carbon-ion beam of 290 MeV/n, and compared with various commercially available plastics using Monte Carlo simulations.

2. Theory

2.1. Measurement of absorbed dose to water in a plastic using an ionization chamber

For absolute dosimetry using a graphite calorimeter, Palmans *et al* (2013) derived a dose conversion formula to obtain dose to water in a water phantom from the measured dose to graphite in a graphite phantom. This formalism was further developed in our previous work (Lourenço *et al* 2016) related to a more practical experimental setup involving measurements in a water phantom, with and without the presence of a graphite absorber in front of the phantom. Here, the formal framework is expanded to derive absorbed dose to water in a water phantom from ionization chamber charge readings performed in a plastic phantom as well as the application of this methodology to carbon-ion beams.

Equations were derived for water, w, which is the standard reference medium in dosimetry, and any plastic material, pl. In this work, $D_A^{(n)}$ is the dose in medium A, calculated using setup number n, and $M^{(n)}$ is the ionization chamber reading for setup n. Three different experimental setups were considered in which doses can be defined and ionization chamber charge readings can be measured, as shown in figure 1:

(i) Setup 1: measurements performed in a water phantom;
(ii) Setup 2: measurements performed in a plastic phantom;
(iii) Setup 3: measurements performed in a water phantom, after passing through a slab of plastic material with thickness t_{pl}.

The determination of absorbed dose to water for a carbon-ion with beam quality Q, using an ionization chamber, is expressed by Andreo *et al* (2000):

$$D_{\mathrm{w}}^{(1)}(z_{\mathrm{w}}^{(1)}) = M^{(1)}(z_{\mathrm{w}}^{(1)}) \,.\, N_{D_{\mathrm{w,Q}}} \tag{1}$$

where $D_{\mathrm{w}}^{(1)}$ is the dose to water in a water phantom, $M^{(1)}$ is the ionization chamber reading in a water phantom and $N_{D_{\mathrm{w,Q}}}$ is the calibration coefficient in terms of absorbed dose to water.

In this work, ionization chamber readings were performed in setups 1 and 3 similarly as by Lourenço *et al* (2016). The distinct advantage of using setup 3 over setup 2 is that only ionization chamber perturbation factors for water are required and values for perturbation factors for the plastic materials are not necessary. The Bragg–Gray cavity theory with a Spencer-Attix stopping power ratio (Attix 1986) is a generic theoretical expression that relates dose-to-medium to dose-to-air in an air cavity under the conditions that the charged particle fluence is not perturbed by the presence of the cavity and no primary charged particles are generated in the cavity. Considering this theory, dose-to-medium, $D_{\mathrm{m}}^{(n)}$, in a given setup n and at a depth of measurement $z_{\mathrm{m}}^{(n)}$, can be related with the ionization in air $M^{(n)}$ by the following expression:

$$D_{\mathrm{m}}^{(n)}(z_{\mathrm{m}}^{(n)}) = M^{(n)}(z_{\mathrm{m}}^{(n)}) \cdot \frac{W_{\mathrm{air}}^{(n)}/e}{m_{\mathrm{air}}} \cdot s_{\mathrm{m,air}}^{\mathrm{SA}}(\Phi_{\mathrm{m}}^{(n)}) \cdot p_{\mathrm{m}}^{(n)}(z_{\mathrm{m}}^{(n)}) \tag{2}$$

where $W_{\mathrm{air}}^{(n)}$ is the mean energy to form an ion pair in air, e is the charge of the electron, m_{air} is the mass of air in the chamber, $s_{\mathrm{m,air}}^{\mathrm{SA}}$ is the medium-to-air Spencer-Attix stopping-power ratio for the fluence in medium m, and $p_{\mathrm{m}}^{(n)}$ the perturbation correction factor for the chamber in medium m to account for deviations from the ideal Bragg–Gray cavity conditions. By application of equation (2) to setups 1 and 3 and considering the ratio of ionization chamber readings between $M^{(1)}$ and $M^{(3)}$, gives:

$$\frac{D_{\mathrm{w}}^{(1)}(z_{\mathrm{w}}^{(1)})}{D_{\mathrm{w}}^{(3)}\left(d^{(3)}, t_{\mathrm{pl}}\right)} = \frac{M^{(1)}(z_{\mathrm{w}}^{(1)})}{M^{(3)}\left(d^{(3)}, t_{\mathrm{pl}}\right)} \cdot \frac{\frac{W_{\mathrm{air}}^{(1)}/e}{m_{\mathrm{air}}}}{\frac{W_{\mathrm{air}}^{(3)}/e}{m_{\mathrm{air}}}} \cdot \frac{s_{\mathrm{w,air}}^{\mathrm{SA}}(\Phi_{\mathrm{w}}^{(1)})}{s_{\mathrm{w,air}}^{\mathrm{SA}}(\Phi_{\mathrm{w}}^{(3)})} \cdot \frac{p_{\mathrm{w}}^{(1)}(z_{\mathrm{w}}^{(1)})}{p_{\mathrm{w}}^{(3)}\left(d^{(3)}, t_{\mathrm{pl}}\right)} \tag{3}$$

where the depth in setup 1, $z_{\mathrm{w}}^{(1)}$, is related to the depth in setup 3, $d^{(3)}$, for the slab t_{pl}, by the water-equivalent thickness of the slab, $t_{\mathrm{pl,w\text{-}eq}}$, all expressed in $\mathrm{g \cdot cm^{-2}}$ (figure 1). The latter is measured experimentally by the difference of ranges in setups 1 and 3, $r^{(1)} - r^{(3)}$, thus, $z_{\mathrm{w}}^{(1)} = d^{(3)} + (r^{(1)} - r^{(3)}) = d^{(3)} + t_{\mathrm{pl,w\text{-}eq}}$. In equation (3), the mass of air in the cavity, m_{air}, drops out because the same chamber was used in setups 1 and 3. The following assumptions are made:

(i) The variation of the mean energy required to reproduce an ion pair, W_{air}/e, between the two setups is negligible (Andreo *et al* 2000). This assumption may introduce considerable

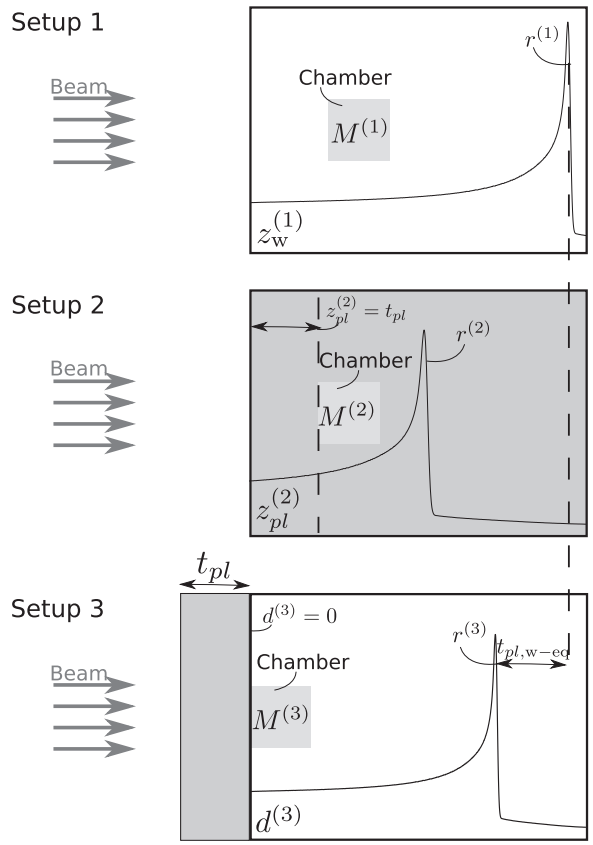

Figure 1. Schematic representation of the experimental setups under consideration. The white colour is used to represent a water phantom, while the dark grey colour represents a plastic phantom in setup 2 and in setups 3 represents plastic slabs with variable thicknesses t_{pl}. Adapted from Lourenço *et al* 2016.

uncertainty, however, currently available data, e.g. from IAEA TRS-398 Code of Practice (Andreo *et al* 2000), suggests no experimental evidence of energy dependence of W_{air}/e for light-ion beams.

(ii) The Spencer-Attix stopping-power ratios vary little with energy, $s_{\mathrm{w,air}}^{\mathrm{SA}}(\Phi_{\mathrm{w}}^{(1)})/s_{\mathrm{w,air}}^{\mathrm{SA}}(\Phi_{\mathrm{w}}^{(3)}) \approx 1$ (Andreo *et al* 2000, Lühr *et al* 2011b).

(iii) The ionization chamber perturbation correction factors are the same for the two setups, $p_{\mathrm{w}}^{(1)}(z_{\mathrm{w}}^{(1)})/p_{\mathrm{w}}^{(3)}(d^{(3)}, t_{\mathrm{pl}}) \approx 1$ since the chamber is always in water and given the slow variation of the perturbation correction factor with energy (Verhaegen and Palmans 2001, Palmans *et al* 2011).

(iv) In the interface between a slab with thickness t_{pl} and the water phantom, $d^{(3)} = 0$ (in setup 3), and when $z_{\mathrm{pl}}^{(2)} = t_{\mathrm{pl}}$ (in setup 2), the ionization chamber reading in setup 3 equals the ionization chamber reading in setup 2, thus, $M^{(3)}(0, t_{\mathrm{pl}}) \approx M^{(2)}(t_{\mathrm{pl}})$; however, $p_{\mathrm{w}}^{(3)}(0, t_{\mathrm{pl}}) \neq p_{\mathrm{pl}}^{(2)}(t_{\mathrm{pl}})$ (figure 1).

Considering the assumptions described above, equation (3) can be rewritten as:

$$\frac{D_{\mathrm{w}}^{(1)}(z_{\mathrm{w}}^{(1)})}{D_{\mathrm{w}}^{(3)}(0,t_{\mathrm{pl}})} \approx \frac{M^{(1)}(z_{\mathrm{w}}^{(1)})}{M^{(3)}(0,t_{\mathrm{pl}})} \approx \frac{M^{(1)}(z_{\mathrm{w}}^{(1)})}{M^{(2)}(t_{\mathrm{pl}})} \tag{4}$$

where the ratio $M^{(1)}(z_{\mathrm{w}}^{(1)})/M^{(2)}(t_{\mathrm{pl}})$ is the fluence scaling factor, h_{pl} (Andreo *et al* 2000). By solving equation (4) for $M^{(1)}$ and inserting the resulting $M^{(1)}$ expression into equation (1), the determination of absorbed dose to water in a plastic can be expressed as:

$$D_{\mathrm{w}}^{(1)}(z_{\mathrm{w}}^{(1)}) \approx M^{(2)}(t_{\mathrm{pl}}) \cdot \frac{M^{(1)}(z_{\mathrm{w}}^{(1)})}{M^{(3)}(0,t_{\mathrm{pl}})} \cdot N_{D_{\mathrm{w,Q}}} \approx M^{(2)}(t_{\mathrm{pl}}) \cdot H_{\mathrm{pl,w}}^{\mathrm{exp}} \cdot N_{D_{\mathrm{w,Q}}} \tag{5}$$

In this work, the term $M^{(1)}(z_{\mathrm{w}}^{(1)})/M^{(3)}(0,t_{\mathrm{pl}})$ is defined as a plastic-to-water conversion factor and will be referred as $H_{\mathrm{pl,w}}$. Using analogous arguments to those related to assumption (iv) described above, $H_{\mathrm{pl,w}} \approx h_{\mathrm{pl}}$.

The $H_{\mathrm{pl,w}}$ term is not an overall conversion factor from dose to plastic in a plastic phantom (setup 2) to dose to water in a water phantom (setup 1) (Palmans *et al* 2013). Instead, $H_{\mathrm{pl,w}}$ relates ionization chamber readings in a plastic phantom (setup 2) with dose to water in a water phantom (setup 1). It can also be interpreted theoretically as relating dose to water in the plastic phantom to dose to water in the water phantom. If $H_{\mathrm{pl,w}} = 1$, no conversion needs to be applied to equation (5) and the plastic material is water-equivalent.

Assuming that the change in fluence between setups 1 and 3 varies little with depth, a mean value of $H_{\mathrm{pl,w}}$ can be calculated for N depths experimentally by a ratio of ionization chamber readings:

$$H_{\mathrm{pl,w}}^{\mathrm{exp}}(t_{\mathrm{pl,w\text{-}eq}}) \approx \frac{1}{N}\sum_{j=1}^{N} \frac{M^{(1)}(z_{\mathrm{w},j}^{(1)})}{M^{(3)}(d_j^{(3)},t_{\mathrm{pl}})} \tag{6}$$

And using Monte Carlo simulations by a ratio of doses,

$$H_{\mathrm{pl,w}}^{\mathrm{MC}}(t_{\mathrm{pl,w\text{-}eq}}) \approx \frac{1}{N}\sum_{j=1}^{N} \frac{D_{\mathrm{w}}^{(1)}(z_{\mathrm{w},j}^{(1)})}{D_{\mathrm{w}}^{(3)}(d_j^{(3)},t_{\mathrm{pl}})} \tag{7}$$

2.2. Relation between $H_{\mathrm{pl,w}}$ and k_{fl}

As derived by Palmans *et al* (2002, 2013), the dose conversion between two media, in this case between water and plastic, can be calculated by:

$$D_{\mathrm{w}}^{(1)}(z_{\mathrm{w\text{-}eq}}) = D_{\mathrm{pl}}^{(2)}\left(z_{\mathrm{pl}}^{(2)}\right) \cdot s_{\mathrm{w,pl}}^{\mathrm{BG}}\left(\Phi_{\mathrm{pl}}^{(2)}\right) \cdot k_{\mathrm{fl}} \tag{8}$$

where $s_{\mathrm{w,pl}}^{\mathrm{BG}}$ is the Bragg–Gray stopping-power ratio for the fluence $\Phi_{\mathrm{pl}}^{(2)}$ and k_{fl} the fluence correction factor. The need for k_{fl} originates from the differences in the non-elastic nuclear interactions between different elements, which result in different particle fluences between water and plastic materials at equivalent depths. Rearranging equation (8), k_{fl} can be calculated by a ratio of doses:

$$k_{\mathrm{fl,dose}}^{\mathrm{MC}} = \frac{D_{\mathrm{w}}^{(1)}(z_{\mathrm{w\text{-}eq}})}{D_{\mathrm{pl}}^{(2)}(z_{\mathrm{pl}}^{(2)}) \cdot s_{\mathrm{w,pl}}^{\mathrm{BG}}(\Phi_{\mathrm{pl}}^{(2)})} \tag{9}$$

It can also be calculated by the ratio of fluences in water and in plastic at equivalent depths (Palmans *et al* 2002, 2013):

$$k^{\mathrm{MC}}_{\mathrm{fl,fluence}}(z_{\mathrm{w\text{-}eq}}) = \frac{\sum_i \left[\int_{E_{\min,i}}^{E_{\max,i}} \Phi^{(1)}_{E,\mathrm{w},i}(E) \cdot \left(\frac{S_i(E)}{\rho} \right)_{\mathrm{w}} \cdot \mathrm{d}E \right]}{\sum_i \left[\int_{E_{\min,i}}^{E_{\max,i}} \Phi^{(2)}_{E,\mathrm{pl},i}(E) \cdot \left(\frac{S_i(E)}{\rho} \right)_{\mathrm{w}} \cdot \mathrm{d}E \right]} \tag{10}$$

where $\Phi_{E,i}$ is the fluence distribution differential in energy for the charged particle type i and S/ρ the mass stopping power. The depth in water, $z^{(1)}_{\mathrm{w}}$, is related to the depth in the phantom material, $z^{(2)}_{\mathrm{pl}}$, by the ratio of ranges in the two materials (Andreo *et al* 2000).

In setup 3, at the interface between a slab of thickness t_{pl} and the water phantom, when $d^{(3)} = 0$, it can also be considered that the fluence will be the same as in setup 2 at $z^{(2)}_{\mathrm{pl}} = t_{\mathrm{pl}}$, i.e. $\Phi^{(3)}_{\mathrm{w}}(0, t_{\mathrm{pl}}) \approx \Phi^{(2)}_{\mathrm{pl}}(t_{\mathrm{pl}})$. This assumption can be applied for carbon-ion beams because secondary particle spectra are mainly from projectile fragmentation. Therefore, they are emitted with similar velocity to the projectile and will have larger ranges, contrary to proton beams where, e.g. alpha particles emitted by target fragmentation with very short ranges have substantial influence (discussed below) (Lourenço *et al* 2016). Thus, dose in setup 3 for $d^{(3)} = 0$ can be written as:

$$D^{(3)}_{\mathrm{w}}(0, t_{\mathrm{pl}}) \approx \sum_i \left[\int_{E_{\min,i}}^{E_{\max,i}} \Phi^{(2)}_{E,\mathrm{pl},i}(E) \cdot \left(\frac{S_i(E)}{\rho} \right)_{\mathrm{w}} \cdot \mathrm{d}E \right] \tag{11}$$

Furthermore, dose in setup 2 is defined as $D^{(2)}_{\mathrm{pl}}(t_{\mathrm{pl}}) = \sum_i \left[\int_{E_{\min,i}}^{E_{\max,i}} \Phi^{(2)}_{E,\mathrm{pl},i}(E) \cdot \left(\frac{S_i(E)}{\rho} \right)_{\mathrm{pl}} \cdot \mathrm{d}E \right]$ for $z^{(2)}_{\mathrm{pl}} = t_{\mathrm{pl}}$. The ratio between dose to water in setup 3 given by equation (11) and dose to plastic in setup 2, gives,

$$\frac{D^{(3)}_{\mathrm{w}}\left(0, t_{\mathrm{pl}}\right)}{D^{(2)}_{\mathrm{pl}}(t_{\mathrm{pl}})} \approx \frac{\sum_i \left[\int_{E_{\min,i}}^{E_{\max,i}} \Phi^{(2)}_{E,\mathrm{pl},i}(E) \cdot \left(\frac{S_i(E)}{\rho} \right)_{\mathrm{w}} \cdot \mathrm{d}E \right]}{\sum_i \left[\int_{E_{\min,i}}^{E_{\max,i}} \Phi^{(2)}_{E,\mathrm{pl},i}(E) \cdot \left(\frac{S_i(E)}{\rho} \right)_{\mathrm{pl}} \cdot \mathrm{d}E \right]} \approx s^{\mathrm{BG}}_{\mathrm{w,pl}}\left(\Phi^{(2)}_{\mathrm{pl}} \right) \tag{12}$$

Thus,

$$D^{(3)}_{\mathrm{w}}\left(0, t_{\mathrm{pl}}\right) \approx D^{(2)}_{\mathrm{pl}}(t_{\mathrm{pl}}) \cdot \; s^{\mathrm{BG}}_{\mathrm{w,pl}}\left(\Phi^{(2)}_{\mathrm{pl}} \right) \tag{13}$$

Combining equation (4) with equation (13):

$$\frac{M^{(1)}(z^{(1)}_{\mathrm{w}})}{M^{(3)}(0, t_{\mathrm{pl}})} \approx \frac{D^{(1)}_{\mathrm{w}}(z^{(1)}_{\mathrm{w}})}{D^{(3)}_{\mathrm{w}}(0, t_{\mathrm{pl}})} \approx \frac{D^{(1)}_{\mathrm{w}}(z^{(1)}_{\mathrm{w}})}{D^{(2)}_{\mathrm{pl}}(t_{\mathrm{pl}}) \cdot s^{\mathrm{BG}}_{\mathrm{w,pl}}(\Phi^{(2)}_{\mathrm{pl}})} \approx k_{\mathrm{fl}}(z_{\mathrm{w\text{-}eq}}) \tag{14}$$

Consequently, $H_{\mathrm{pl,w}} \approx k_{\mathrm{fl}}$. In previous work (Lourenço *et al* 2016), the ratio of ionization chamber readings between setups 1 and 3 was used to obtain fluence corrections experimentally in clinical proton beams. The results showed that fluence corrections obtained experimentally, accounted for the primary and part of the secondary particle spectra and, therefore, represented partial fluence corrections. Indeed, in proton beams, the energy of alpha particles, emitted by target fragmentation, is not sufficient to penetrate the wall of the ionization chamber and these particles are not accounted for in the experimental fluence correction factor. A correction factor F was established to relate fluence corrections defined theoretically

to partial fluence corrections measured experimentally. However, in the case of a high-energy carbon-ion beam, the energies of secondary projectile fragments are large enough to cross the chamber wall (Haettner *et al* 2013) and fluence corrections obtained from experiments will thus include all charged particles, i.e. $F = 1$ and $\Phi_{\mathrm{w}}^{(3)}(0, t_{\mathrm{pl}}) \approx \Phi_{\mathrm{pl}}^{(2)}(t_{\mathrm{pl}})$, with the exception of heavy particles from target fragmentation which are less abundant in these beams.

In summary, $H_{\mathrm{pl,w}}^{\mathrm{exp}}$ factors were measured experimentally from equation (6) and $H_{\mathrm{pl,w}}^{\mathrm{MC}}$ and $k_{\mathrm{fl}}^{\mathrm{MC}}$ factors were calculated using Monte Carlo simulations from equations (7), (9) and (10), respectively.

3. Materials and methods

3.1. Water-equivalent plastics

The plastic materials prepared in this work consist of epoxy resins and were produced in collaboration with the St Bartholomew's Hospital, UK, based on earlier experience from White (1978), White *et al* (1977, 1980) and Constantinou *et al* (1982). Epoxy resins consist of low-molecular-weight compounds containing epoxide groups. Compounds containing a reactive group to the epoxide (a.k.a. hardeners), when mixed together with the epoxy resin, produce a linked polymer that can be mixed with powders of different compositions. The resulting plastic is a rigid material and insoluble in water.

Three plastic materials were produced based on the same epoxy resin system (epoxy resin + hardener). Powders with varying atomic low-Z numbers were added to the resin in order to change the atomic number of the final compound. Here, the plastics will be referred as plastics #1, #2 and #3, respectively. Gas-filled spheres called phenolic microspheres (PMS), 50 μm thick, were added in the composition of the resin in order to adjust the density of the final compound to approximately $1\,\mathrm{g}\cdot\mathrm{cm}^{-3}$. For each plastic formulation, three slabs of 4 cm, 5 cm and 8 cm thick were machined from the same batch.

3.2. Measurements

The plastic-to-water conversion factor $H_{\mathrm{pl,w}}^{\mathrm{exp}}$ was measured for the three novel plastics. Measurements were performed in the clinical carbon synchrotron at the Gunma University Heavy Ion Medical Center (GHMC), Japan (Ohno *et al* 2011). A 290 MeV/n carbon-ion beam was provided by a wobbling delivery system (Komori *et al* 2004, Yonai *et al* 2008) which magnetically scanned the scattered beam.

Measurements were performed in a broad collimated field of $11 \times 11\,\mathrm{cm}^2$ without beam modulation. A cylindrical Farmer ionization chamber (PTW type 30011) was placed in the corner of the beam exit in order to monitor the beam. Central axis measurements were performed using a plane-parallel Roos ionization chamber (PTW type 34001) with a sensitive diameter of 1.5 cm. The Roos chamber was kept at a constant source-to-detector distance (SDD), in order to avoid corrections for the divergence of the beam. A water phantom was placed in front of the beam, with the phantom surface aligned with the isocenter. The water phantom was moved towards the beam in order to change the amount of water in front of the static Roos chamber. This was repeated with slabs of water-equivalent plastics of variable thicknesses attached to the front window of the water phantom. Finally, for each slab of plastic tested with thickness t_{pl}, $H_{\mathrm{pl,w}}^{\mathrm{exp}}$ was determined by application of equation (6).

Table 1. Experimental relative standard uncertainties.

Sources of uncertainty	Type A (%)	Type B (%)
Standard/monitor ratio	0.32	—
Temperature	—	0.05
Pressure	—	0.05
$s_{[H_{\mathrm{pl,w}}^{\overline{\mathrm{exp}}}]}$	—	0.16
Overall	**0.32**	**0.18**
Combined (%)	**0.37**	

3.3. Monte Carlo simulations

Monte Carlo simulations were performed with the FLUKA code version 2011.2c.3 (Ferrari *et al* 2005, Böhlen *et al* 2014). To calculate $H_{\mathrm{pl,w}}^{\mathrm{MC}}$ using equation (7), depth-dose distributions were calculated in water (setup 1) and in water after passing through slabs of plastic with variable thickness (setup 3). The simulated slabs had the same thickness and density of those tested experimentally. For comparison with $H_{\mathrm{pl,w}}^{\mathrm{MC}}$, $k_{\mathrm{fl}}^{\mathrm{MC}}$ was also calculated using the dose and the fluence approaches, from equations (9) and (10), respectively. Fluence differentials in energy and dose were scored in bins of 0.1 cm and 0.007 cm thick, respectively, within cylindrical volumes of 1.5 cm diameter (equal to the sensitive diameter of the Roos chamber used in the experiments). For each simulation, 25×10^6 particles were simulated for a broad carbon-ion beam of $11 \times 11\,\mathrm{cm}^2$. A beam with no divergence was considered in the simulations because it corresponded to a better approximation of the experiments performed with constant SDD.

Commercially available plastics were also simulated by Monte Carlo for comparison with the three trial compositions of water-equivalent plastics characterized in this work. The following plastics were included: A-150, PMMA, polyethylene, polystyrene, RANDO® phantom soft tissue (The Phantom Laboratory, Salem, NY, USA), Plastic Water® (CIRS, Norfolk, VA, USA), RMI-457 (GAMMEX, Middleton, WI, USA), Virtual Water™ (Med-Cal, Middleton, WI, USA), Gammex 457-CTG (CTG Solid Water®: GAMMEX, Middleton, WI, USA) and WT1 (St Bartholomew's Hospital, London, UK). Existing plastics were defined in terms of elemental mass fractions, density and mean excitation energy (a.k.a. *I*-value) as stated in ICRU Reports 37 (1984) and 49 (1993) and IAEA TRS-398 Code of Practice (Andreo *et al* 2000). When experimentally determined *I*-values were not available, *I*-values were obtained by the application of the Bragg additivity rule for compounds (ICRU 1984).

3.4. Experimental and Monte Carlo uncertainties

The sources of experimental uncertainties to determine $H_{\mathrm{pl,w}}^{\mathrm{exp}}$ are presented in table 1 (JCGM 2008). Type A uncertainties were calculated as one standard deviation of the mean of repeated observations. Type B uncertainties included temperature and pressure and standard deviation of the mean values $H_{\mathrm{pl,w}}^{\mathrm{exp}}$ at all calculated depths. Ratios of ionizations were measured (standard chamber/monitor chamber) with the same type of electrometer, therefore, type B uncertainties related to electrometer calibrations were correlated and cancelled out. Uncorrelated uncertainties, such as fluctuations and drifts, were considered negligible for the electrometer used. Uncertainties related to the determination of equivalent depths between setups 1 and 3 were also considered negligible. This becomes mainly a large uncertainty close to the Bragg

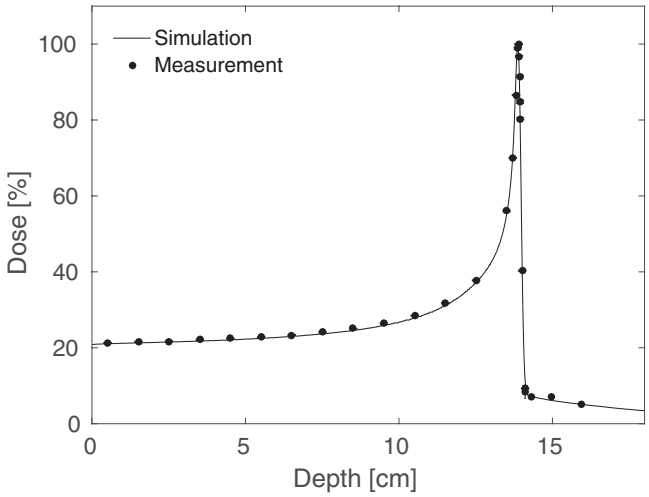

Figure 2. Measured and simulated depth-dose curves in water. Experimental error bars are smaller than the marker points.

peak because of the high sensitivity to positioning errors in depth. Therefore, those points were not considered in equations (6) and (7) to calculate $H_{\mathrm{pl,w}}$.

Type A uncertainties from Monte Carlo simulations were below 0.3% and type B uncertainties were not considered. Type B Monte Carlo uncertainties are more challenging to estimate than type A. Type B Monte Carlo uncertainties include uncertainties from stopping-power data and interaction cross sections. Böhlen *et al* (2010) conducted a study to benchmark nuclear models implemented in FLUKA for carbon-ion beams. The authors concluded that FLUKA code predicted experimental data with reasonable accuracy, although further improvements were needed since the existing experimental data was limited and had large uncertainties. Stopping powers from different models were compared with experimental data in ICRU Report 73 (ICRU 2005). Overall, data agreed to within 10% with higher accuracy for energies above 10 MeV/n, however, for energies below 0.1 MeV/n, uncertainties were larger due to considerable disagreement between experimental data and models (ICRU 2005). Note that in equation (10) the same stopping power data are used in the numerator and denominator, therefore, the correlation in these uncertainties is large and cancel out. Although in equation (9) the uncertainty contribution from the stopping-power ratio has a large influence, it will be strongly correlated with the ratio of calculated doses (Palmans *et al* 2013).

4. Results and discussion

4.1. Tuning of the beam model and benchmarking of the simulations

Monte Carlo simulations were first validated against experimental data and results in the literature. In Monte Carlo, both the beam energy and the Gaussian energy spread were tuned to achieve good agreement between the experimental and simulated Bragg peak curves. This correction resulted in a mean beam energy of 265 MeV/n with a standard deviation of $\sigma = 0.75$ MeV incident at the phantom surface. In figure 2, a relative dose curve as a function of measurement depth acquired during the experiments is compared with a depth-dose distribution

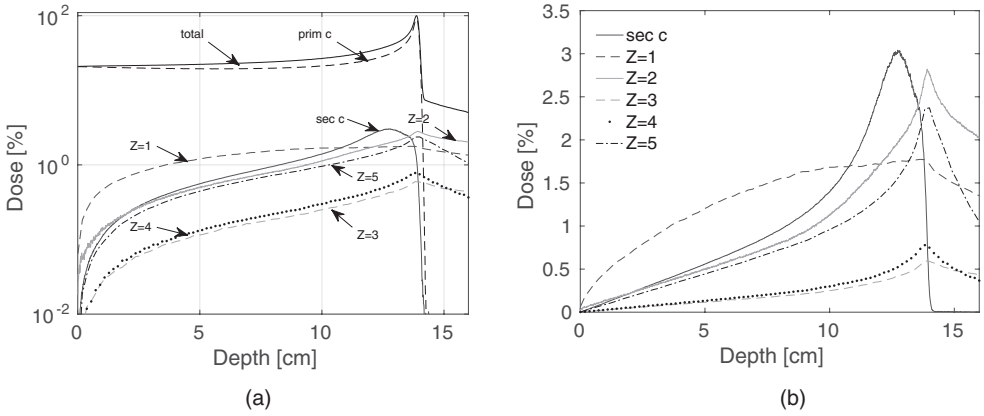

Figure 3. Monte Carlo simulations of absorbed dose curves as a function of depth in water, for different set of particles (prim c = primary particles, sec c = secondary carbon ions, and particles with atomic numbers $Z = 1$, $Z = 2$, $Z = 3$, $Z = 4$ and $Z = 5$).

from Monte Carlo simulations. The assumption is made that ionization in the chamber is proportional to dose (equation (4)). Both distributions were normalized to the integral of the curves. The tail beyond the Bragg peak is due to the fragmentation of primary carbon ions which produces secondary particles with a smaller mass and similar velocity to the projectile. Consequently, these lighter fragments will deposit their energy at a depth beyond the Bragg peak, to which mostly lighter fragments ($1 \leqslant Z \leqslant 2$) contribute.

Figure 3 shows the contribution of primary and secondary particles in water. The following particles were scored: primary carbon ions, secondary particles with $Z = 1$ (protons, deuterons, tritons), $Z = 2$ (isotopes of helium ^{3}He, ^{4}He), $Z = 3$ (isotopes of lithium ^{6}Li, ^{7}Li), $Z = 4$ (isotopes of beryllium ^{7}Be, ^{9}Be, ^{10}Be), $Z = 5$ (isotopes of boron ^{12}B, ^{13}B) and $Z = 6$ (isotopes of carbon ^{10}C, ^{11}C, ^{12}C). Other isotopes and neutrons with a contribution to the dose of the order of 0.001% were not scored. Unlike fragments, primary particles do not contribute to the tail dose shown in figure 3(a). The contribution of fragments increases in depth and a maximum is reached in the Bragg peak. Beyond the Bragg peak their contribution decreases gradually because there are no primary particles producing secondary particles. Haettner *et al* (2013) measured experimentally dose distributions in water originating from secondary charged particles for 200 MeV/n and 400 MeV/n carbon-ion beams, while Kempe *et al* (2007) and Rossomme *et al* (2013) calculated dose distributions in water originating from primary and secondary charged particles for a 391 MeV/n carbon-ion beam using SHIELD-HIT code and for an 80 MeV/n carbon-ion beam using Geant4/Gate codes, respectively. Experimental data from Haettner *et al* (2013) showed that fragments with $Z = 1$ (hydrogen nuclei) and $Z = 2$ (helium nuclei) have a larger contribution to the dose than fragments with $Z = 3$ (lithium nuclei), $Z = 4$ (beryllium nuclei), and $Z = 5$ (boron nuclei). However, larger uncertainties were reported for fragments with $Z = 5$. Our results are in agreement with their findings, with the exception of fragments with $Z = 5$, where a contribution of the same order of magnitude as for $Z = 1$ and $Z = 2$ was found. Previous Monte Carlo studies from Kempe *et al* (2007) and Rossomme *et al* (2013) show similar results to ours. The latter reported a discontinuity in the depth dose curve for $Z = 2$ fragments using Geant4 and concluded it could be the result of artefacts due to the implementation of interaction cross sections. In our case, using FLUKA, depth-dose distributions from all fragments follow a smooth curve.

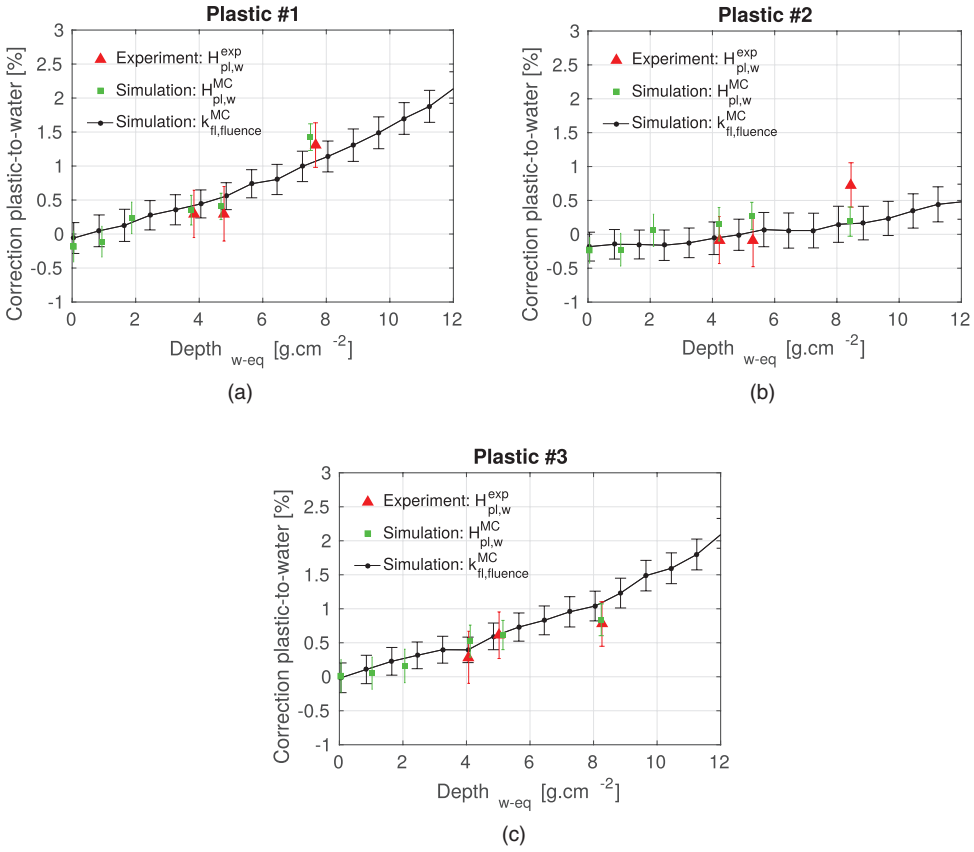

Figure 4. Plastic-to-water corrections for three trial compositions of water-equivalent plastics: (a) plastic #1, (b) plastic #2 and (c) plastic #3. Triangles represent the values of $H^{exp}_{pl,w}$ calculated experimentally (refer to equation (6)), squares represent the values of $H^{MC}_{pl,w}$ calculated using Monte Carlo methods (equation (7)) and circles represent the values of $k^{MC}_{fl,fluence}$ (refer to equation (10)).

4.2. Plastic-to-water conversion factor

Figure 4 shows the plastic-to-water conversion factor for the three novel plastics characterized experimentally. In the graphs, data are included that were obtained from experiments, $H^{exp}_{pl,w}$, and from Monte Carlo simulations, $H^{MC}_{pl,w}$. For comparison, the results from k^{MC}_{fl} are also shown. Results from $H_{pl,w}$ and k_{fl} factors for the different plastics are shown as percent corrections in comparison to water. The approaches $k^{MC}_{fl,fluence}$ and $k^{MC}_{fl,dose}$ are strongly linked (0.05% difference) (Palmans *et al* 2013) and the results between methods were consistent. For simplification, the results from the latter have not been included in the graphs.

For plastic #1, average differences between experimental data and numerical simulations were of the order of 0.20% for $k^{MC}_{fl,fluence}$ and 0.10% for $H^{MC}_{pl,w}$. Differences were larger for plastic #2, where mean values were 0.24% and 0.38% for $k^{MC}_{fl,fluence}$ and $H^{MC}_{pl,w}$, respectively. For plastic #3, average differences between experimental data and numerical simulations were of the order of 0.15% for $k^{MC}_{fl,fluence}$ and 0.10% for $H^{MC}_{pl,w}$. The production process of plastics has uncertainties and the assumed compositions may not always be consistent with the ones

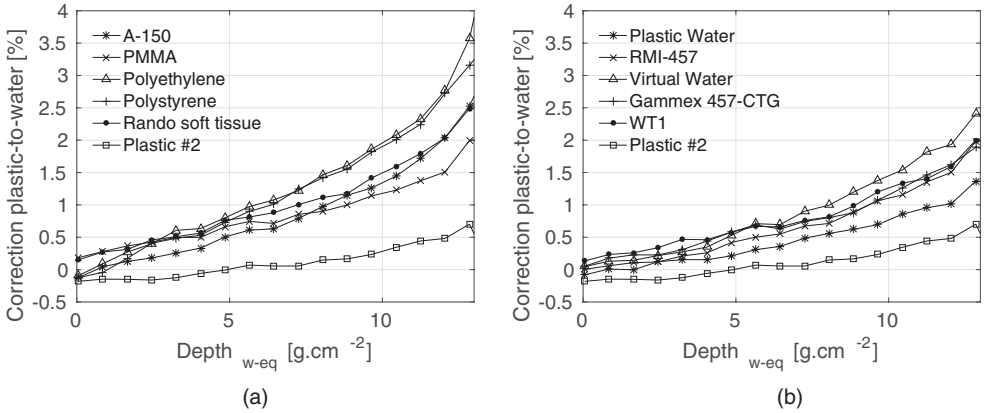

Figure 5. Dose conversion corrections from plastic-to-water for various commercially available plastic materials and for plastic #2.

produced. The latter may explain small discrepancies between experimental and numerical methods. Nevertheless, these results suggest that $H_{\mathrm{pl,w}}^{\mathrm{exp}}$, obtained experimentally from setups 1 and 3, account for all charged particles and ensure the validity of the assumptions considered. The good agreement between $H_{\mathrm{pl,w}}^{\mathrm{MC}}$ and $k_{\mathrm{fl}}^{\mathrm{MC}}$ implies that they are comparable. The latter is easier to implement in Monte Carlo since a single simulation is enough to calculate $k_{\mathrm{fl}}^{\mathrm{MC}}$ with depth, whereas $H_{\mathrm{pl,w}}^{\mathrm{MC}}$ requires a simulation for each thickness of material in order to obtain its variation with depth.

Experimental data showed no preference regarding the most water-equivalent plastic with measured $H_{\mathrm{pl,w}}^{\mathrm{exp}}$ values amounting to a maximum of 0.8% for plastic #1, while for plastic #2 and plastic #3 a maximum correction of 0.7% and 1.3% was found, respectively. Considering the results from Monte Carlo simulations, for plastics #1 and #3, $H_{\mathrm{pl,w}}^{\mathrm{MC}}$ increased towards 2% at a depth near the Bragg peak, while for plastic #2 it increased gradually towards 0.5% with depth. The different rate of variation of $H_{\mathrm{pl,w}}^{\mathrm{MC}}$ with depth between the different plastics suggest that varying the concentration of an additive to the epoxy resin system enables the properties of the materials to be altered towards water-equivalence.

In figure 5, plastic #2 is compared with various commercially available plastic materials, using Monte Carlo simulations since only a limited amount of experimental data is available in the literature. Moreover, the maximum difference between Monte Carlo and experimental data for the three in-house plastics in figure 4 was 0.57%. For this purpose, $k_{\mathrm{fl,fluence}}^{\mathrm{MC}}$ was calculated due to its easy implementation in Monte Carlo. For polyethylene, polystyrene, A-150 and Rando phantom soft tissue the correction increased from 0% to 2.5%–4.0% at a depth near the Bragg peak, while for PMMA it increased towards 2%. Water-equivalent plastics such as, Plastic Water, RMI-457, Gammex 457-CTG, WT1 and Virtual Water, gave similar results, where maximum corrections were of the order of 1.5%–2.5%. Plastic #2 gave the most promising results with $k_{\mathrm{fl,fluence}}^{\mathrm{MC}}$ varying between 0.0%–0.5% with depth. Similar results were found by Lühr *et al* (2011a) for PMMA. The latter performed a Monte Carlo study, using SHIELD-HIT10A code, to determine fluence corrections for PMMA in comparison to water in 107 MeV/n, 270 MeV/n and 400 MeV/n carbon-ion beams. For the 107 MeV/n carbon-ion beam, corrections were close to unity, while for the higher-energy beams corrections deviated from unity by 0% at the surface to 1%–2% at a depth near the Bragg peak.

5. Conclusions

In this work, a plastic-to-water conversion factor, $H_{pl,w}$, was established to derive absorbed dose to water in a water phantom from ionization chamber readings performed in a plastic phantom for carbon ion-beams. Three trial plastic materials with varying atomic compositions were produced based on epoxy resins, and characterized experimentally in a high-energy carbon-ion beam. Experimental data showed no preference regarding the most water-equivalent plastic with measured $H_{pl,w}^{exp}$ values amounting to a maximum of 0.7%–1.3%. Considering the results from Monte Carlo simulations, the good agreement between $H_{pl,w}^{MC}$ and k_{fl}^{MC} suggested that they are comparable. For plastics #1 and #3 it was found that the simulated plastic-to-water correction increased towards 2% at a depth near the Bragg peak, while for plastic #2 the correction increased gradually towards 0.5%. Plastic #2 was found to be superior to plastics commercially available with a k_{fl}^{MC} correction 1.0–3.5% smaller at larger depths.

This work presents a proof-of-principle that varying the concentration of an additive to the epoxy resin system alters the properties of the plastics towards water-equivalence. This work will feed into the development of water- and tissue-equivalent materials for light-ion beams. Future work will focus on the characterization of the novel plastics in low- and high-energy proton beams.

Acknowledgments

The authors would like to thank James Renaud and Séverine Rossomme for their assistance during the experiments and Simon Duane for useful discussions and feedback on the manuscript. The authors acknowledge the use of the UCL Legion High Performance Computing Facility (Legion@UCL), and associated support services, in the completion of this work, and the FLUKA mailing list for all the support with FLUKA code. AL was supported by University College London and the UK National Physical Laboratory through the National Measurement System.

References

Al-Sulaiti L, Palmans H, Thomas R A S, Shipley D and Kacperek A 2010 Water equivalence of A150, aluminium and copper in a low-energy clinical proton beam *Nucl. Instrum. Methods Phys. Res.* A **619** 344–7

Al-Sulaiti L, Shipley D, Thomas R, Owen P, Kacperek A, Regan P H and Palmans H 2012 Water equivalence of some plastic-water phantom materials for clinical proton beam dosimetry *Appl. Radiat. Isot.* **70** 1052–5

Andreo P, Burns D T, Hohlfeld K, Huq M S, Kanai T, Laitano F, Smyth V G and Vynckier S 2000 *Absorbed Dose Determination in External Beam Radiotherapy: an International Code of Practice for Dosimetry Based on Standards of Absorbed Dose to Water* (*IAEA Technical Report Series 398*) (Vienna: IAEA)

Attix F H 1986 *Introduction to Radiological Physics and Radiation Dosimetry* (New York: Wiley)

Böhlen T T, Cerutti F, Chin M P W, Fassò A, Ferrari A, Ortega P G, Mairani A, Sala P R, Smirnov G and Vlachoudis V 2014 The FLUKA Code: developments and challenges for high energy and medical applications *Nucl. Data Sheets* **120** 211–4

Böhlen T T, Cerutti F, Dosanjh M, Ferrari A, Gudowska I, Mairani A and Quesada J M 2010 Benchmarking nuclear models of FLUKA and GEANT4 for carbon ion therapy *Phys. Med. Biol.* **55** 5833–47

Constantinou C, Attix F H and Paliwal B R 1982 A solid water phantom material for radiotherapy x-ray and gamma-ray beam calibrations *Med. Phys.* **9** 436–41
Ding G X, Rogers D W O, Cygler J E and Mackie T R 1997 Electron fluence correction factors for conversion of dose in plastic to dose in water *Med. Phys.* **24** 161–76
Ferrari A, Sala P R, Fassò A and Ranft J 2005 FLUKA: a multi-particle transport code CERN-2005-10, INFN/TC_05/11, SLAC-R-773
Haettner E, Iwase H, Krämer M, Kraft G and Schardt D 2013 Experimental study of nuclear fragmentation of 200 and 400 MeV/u (12)C ions in water for applications in particle therapy *Phys. Med. Biol.* **58** 8265–79
ICRU 1984 *Stopping Powers for Electrons and Positions* (*ICRU Report 37*) (Bethesda, MD: ICRU)
ICRU 1993 *Stopping Powers and Ranges for Protons and Alpha Particles* (*ICRU Report 49*) (Bethesda, MD: ICRU)
ICRU 2005 *Stopping of Ions Heavier than Helium* (*ICRU Report 73*) (Bethesda, MD: ICRU)
Inaniwa T, Kanematsu N, Hara Y and Furukawa T 2015a Nuclear-interaction correction of integrated depth dose in carbon-ion radiotherapy treatment planning *Phys. Med. Biol.* **60** 421–35
Inaniwa T, Kanematsu N, Tsuji H and Kamada T 2015b Influence of nuclear interactions in body tissues on tumor dose in carbon-ion radiotherapy *Med. Phys.* **42** 7132
Joint Committee for Guides in Metrology (JCGM) 2008 Evaluation of measurement data—Guide to the expression of uncertainty in measurement JCGM 100:2008
Kanematsu N, Koba Y and Ogata R 2013 Evaluation of plastic materials for range shifting, range compensation, and solid phantom dosimetry in carbon-ion radiotherapy *Med. Phys.* **40** 041724
Kanematsu N, Koba Y, Ogata R and Himukai T 2014 Influence of nuclear interactions in polyethylene range compensators for carbon-ion radiotherapy *Med. Phys.* **41** 071704
Kempe J, Gudowska I and Brahme A 2007 Depth absorbed dose and LET distributions of therapeutic 1H, 4He, 7Li, and 12C beams *Med. Phys.* **34** 183–92
Khan F M, Doppke K P, Hogstrom K R, Kutchner G J, Nath R, Prasad S C, Purdy J A, Rozenfeld M and Werner B L 1991 Clinical electron-beam dosimetry: report of AAPM Radiation Therapy Committee Task Group No 25 *Med. Phys.* **18** 73–109
Komori M, Furukawa T and Kanai T 2004 Optimization of spiral-wobbler system for heavy-ion radiotherapy *Japan. J. Appl. Phys.* **43** 6463–7
Lourenço A, Thomas R, Bouchard H, Kacperek A, Vondracek V, Royle G and Palmans H 2016 Experimental and Monte Carlo studies of fluence corrections for graphite calorimetry in low- and high-energy clinical proton beams *Med. Phys.* **43** 4122–32
Lühr A, Hansen D C, Sobolevsky N, Palmans H, Rossomme S and Bassler N 2011a Fluence correction factors and stopping power ratios for clinical ion beams *Acta Oncol.* **50** 797–805
Lühr A, Hansen D C, Jäkel O, Sobolevsky N and Bassler N 2011b Analytical expressions for water-to-air stopping-power ratios relevant for accurate dosimetry in particle therapy *Phys. Med. Biol.* **56** 2515–33
McEwen M and DuSautoy A R 2003 Characterisation of the water-equivalent material Wte for use in electron beam dosimetry *Phys. Med. Biol.* **48** 1885–93
Ohno T *et al* 2011 Carbon ion radiotherapy at the Gunma University Heavy Ion Medical Center: new facility setup *Cancers* **3** 4046–60
Paganetti H 2009 Dose to water versus dose to medium in proton beam therapy *Phys. Med. Biol.* **54** 4399–421
Palmans H, Al-Sulaiti L, Andreo P, Shipley D, Lühr A, Bassler N, Martinkovič J, Dobrovodský J, Rossomme S, Thomas R A S 2013 Fluence correction factors for graphite calorimetry in a low-energy clinical proton beam: I. Analytical and Monte Carlo simulations *Phys. Med. Biol.* **58** 3481–99
Palmans H, Al-Sulaiti L, Andreo P, Thomas R A S, Shipley D R S, Martinkovič J and Kacperek A 2011 Conversion of dose-to-graphite to dose-to-water in a clinical proton beam *Standards, Applications and Quality Assurance in Medical Radiation Dosimetry* (*Proceedings of an International Symposium* vol 1) (IAEA, Vienna, Austria) pp 343–55
Palmans H, Symons J E, Denis J-M, de Kock E A, Jones D T L and Vynckier S 2002 Fluence correction factors in plastic phantoms for clinical proton beams *Phys. Med. Biol.* **47** 3055–71
Palmans H and Verhaegen F 1997 Calculated depth dose distributions for proton beams in some low-*Z* materials *Phys. Med. Biol.* **42** 1175–83

Palmans H and Verhaegen F 2005 Assigning nonelastic nuclear interaction cross sections to Hounsfield units for Monte Carlo treatment planning of proton beams *Phys. Med. Biol.* **50** 991–1000

Rossomme S, Palmans H, Shipley D, Thomas R, Lee N, Romano F, Cirrone P, Cuttone G, Bertrand D and Vynckier S 2013 Conversion from dose-to-graphite to dose-to-water in an 80 MeV/A carbon ion beam *Phys. Med. Biol.* **58** 5363–80

Seuntjens J, Olivares M, Evans M and Podgorsak E 2005 Absorbed dose to water reference dosimetry using solid phantoms in the context of absorbed-dose protocols *Med. Phys.* **32** 2945–53

Thwaites D I 1985 Measurements of ionisation in water, polystyrene and a 'solid water' phantom material for electron beams *Phys. Med. Biol.* **30** 41–53

Verhaegen F and Palmans H 2001 A systematic Monte Carlo study of secondary electron fluence perturbation in clinical proton beams (70–250 MeV) for cylindrical and spherical ion chambers *Med. Phys.* **28** 2088–95

Vynckier S, Bonnett D E and Jones D T L 1991 Code of practice for clinical proton dosimetry *Radiother. Oncol.* **20** 53–63

White D R 1978 Tissue substitutes in experimental radiation physics *Med. Phys.* **5** 467–79

White D R, Martin R J and Darlison R 1977 Epoxy resin-based tissue substitutes *Br. J. Radiol.* **50** 814–21

White D R and Tucker A K 1980 A test object for assessing image quality in mammography *Br. J. Radiol.* **53** 331–5

Yonai S, Kanematsu N, Komori M, Kanai T, Takei Y, Takahashi O, Isobe Y, Tashiro M, Koikegami H and Tomita H 2008 Evaluation of beam wobbling methods for heavy-ion radiotherapy *Med. Phys.* **35** 927–38

Zhang R, Taddei P J, Fitzek M M and Newhauser W D 2010 Water equivalent thickness values of materials used in beams of protons, helium, carbon and iron ions *Phys. Med. Biol.* **55** 2481–93